This is an *Accepted Manuscript*, which has been through the Royal Society of Chemistry peer review process and has been accepted for publication.

Accepted Manuscripts are published online shortly after acceptance, before technical editing, formatting and proof reading. Using this free service, authors can make their results available to the community, in citable form, before we publish the edited article. We will replace this *Accepted Manuscript* with the edited and formatted *Advance Article* as soon as it is available.

You can find more information about *Accepted Manuscripts* in the **Information for Authors**.

Journal Name

ARTICLE

Hierarchical importance of coordination and hydrogen bonds in the formation of homochiral 2D coordination polymers and 2D supramolecular assemblies

Navnita Kumar[a], Sadhika Khullar[a,¶] Yogesh Singh[b] and Sanjay K. Mandal[a,*]

In exploring the chemistry of reduced Schiff base derivatives of amino acids with Cu(II) ion, a series of homochiral two-dimensional (2D) coordination polymer (CP) with a unique loop-like structure comprised of five Cu(II) centers, $\{[Cu_2(Hsersal)_2(H_2O)]^.H_2O\}_n$, (**1**), $\{[Cu_2(Hser-5OMe-sal)_2(H_2O)]^.DMF\}_n$ (**2**), $\{[Cu_2(Hser-5NO_2-sal)_2(H_2O)]^.2H_2O\}_n$ (**3**), $\{[Cu_2(Hser-5Cl-sal)_2(H_2O)]^.2H_2O\}_n$ (**4**), $\{[Cu_2(Hser-3Cl-sal)_2(H_2O)]^.3H_2O\}_n$ (**5**) and $\{[Cu_2(Hser-o-Van)_2(H_2O)]^.3H_2O\}_n$ (**6**) [where H_3sersal = N-(2-hydroxybenzyl)-serine, H_3ser-5OMe-sal = N-(2-hydroxy-5-methoxybenzyl)-serine, H_3ser-5NO$_2$-sal = N-(2-hydroxy-5-nitrobenzyl)-serine, H_3ser-5-Cl-sal = N-(2-hydroxy-5-chlorobenzyl)-serine, H_3ser-3-Cl-sal = N-(2-hydroxy-3-chlorobenzyl)-serine, H_3ser-o-van = N-(2-hydroxy-3-methoxybenzyl)-serine], have been isolated in good yields from the reaction of a methanolic solution of $CuSO_4^.5H_2O$ and potassium salt of the respective ligands (in a 1:1 ratio) either at room temperature or under reflux. In these CPs, the two Cu(II) centers have different coordination environments with one coordinated to a water molecule. Using a bifunctional linker, such as 4,4'-bipyridine, four of these 2D CPs are converted in methanol under reflux to the corresponding 2D supramolecular coordination complexes (SCCs) constructed through very strong hydrogen bonding interactions, $[Cu_2(4,4'-bpy)(Hsersal)_2]^.2H_2O$ (**7**), $[Cu_2(4,4'-bpy)(Hser-5-OMe-sal)_2]^.6H_2O$ (**8**), $[Cu_2(4,4'-bpy)(Hser-5-NO_2-sal)_2]^.H_2O$ (**9**) and $[Cu_2(4,4'-bpy)(Hser-5-Cl-sal)_2]^.4H_2O^.DMF$ (**10**). This chemical conversion of a CP to an SCC is unknown in the literature and indicates the hierarchical importance of coordination and hydrogen bonds in their formation. These are structurally characterized by elemental analysis, UV-Vis, circular dichroism, IR and Raman spectroscopy, ESI mass spectrometry, single crystal and powder X-ray diffraction, polarimetry and thermogravimetric analysis. A magneto-structural correlation for the change from **1** to **7** is established through variable temperature magnetic susceptibility measurements (2-380 K) indicating strong antiferromagnetic coupling ($2J = -278$ cm^{-1}) in **1** and no interaction in **7** between the Cu(II) centers. As an example, water adsorption studies of **1** and **7** were carried out to demonstrate the porous nature of the SCCs compared to the CPs.

Introduction

In the last few decades design, synthesis and structural characterization of Coordination Polymers (CPs) and Supramolecular Coordination Complexes (SCCs), two subsets of Metal Organic Coordination Networks (MOCNs), have been the subject of immense interest for their important roles in various applications, such as catalysis, luminescence, molecular separation, gas and liquid adsorption, non-linear optics, etc.[1-5] Further association of the 1D or 2D CPs, constructed by coordination bonds, through strong and/or weak hydrogen bonds, π-π stacking of aromatic moieties or C-H…O

interactions, etc., also generates supramolecular assemblies of higher dimensions with open networks. Thus, hydrogen-bonded MOCNs comprised of CPs use both coordination bonds and hydrogen bonds in their construction with major contribution arising from the former type of bonds. On the other hand, the construction of SCCs of higher dimensionality through the stepwise assembly process that starts with the association of discrete precursors, such as monomers and dimers, by strong supramolecular interactions has been found to be a powerful strategy. This variation in the contribution of the coordination bonds and hydrogen bonds has been the key to making diverse (structural and functional) MOCNs in recent years.[6-11] While

these two bonding are orthogonal in nature, the formation of CPs over SCCs and vice versa could be due to the hierarchical importance of these two forces in the overall structure. Through judicious choice of the components in making MOCNs, it is possible to generate materials with tunable structures and properties.

Using various synthetic methods MOCNs are prepared from a variety of metal centers or metal atom clusters and multi-atom organic linkers. Due to the chiral nature of amino acid based ligands, MOCNs made thereof can be used in enantiomeric separation, drug purification, asymmetric catalysis, etc. The use of amino acids in making the chiral ligands is preferred not only due to their low cost and easy availability but also for their abilities to act both as hydrogen bond donors and acceptors. The various functionalities present in these ligands, e.g., carboxylate, hydroxy, etc., also show different binding modes with the metal centers.[12-14] Utilizing the reduced Schiff base ligands of various amino acids, numerous CPs and SCCs have been reported in the literature.[15] Specifically, dinuclear metal complexes with bis(alkoxo) or bis(phenoxo) cores have been studied for their use in this regard. For example, the metal complexes of Cu(II), Zn(II), Ni(II), etc., containing N-(2-hydroxybenzyl)-amino acid ligands [e. g., N-(2-hydroxybenzyl)-L-alanine, N-(2-hydroxybenzyl)-L-valine, N-(2-hydroxybenzyl)-L-tyrosine, N-(2-hydroxybenzyl)-L-tryptophan, N-(2-hydroxybenzyl)-L-glycine] of the general formula M_2L_2 have been studied in detail.[16-20] However, no structural diversity was observed due to a variation of the components used in making such CPs and SCCs.

Interconversions of CPs to SCCs allow one to understand the structure and bonding in these species and to provide further directions in the rational design of improved materials. The topochemical conversion of SCCs comprised of the M_2L_2 type mentioned above to the corresponding CPs by thermal dehydration has been reported several years ago.[17,18] In these examples, the CPs are formed with the removal of coordinated solvent molecules upon thermal treatment for the available carboxylate groups to bridge between the metal centers. To the best of our knowledge, there is no example of conversion of a CP to the corresponding SCC reported in the literature. Thus we initiated our work to successfully make several 2D CPs of divalent metal ions, such as Cu(II), with serine based Schiff based ligands where the CH_2OH side-arm of the ligands was found to play a huge role in their formation. Furthermore, we have achieved in converting the non-porous CPs to porous SCCs which are associated with tunable properties. In doing so, we also show the evidence for the important role played by hydrogen bonding in the stabilization of the SCCs.

In the present study we report a series of 2D CPs with a unique loop-like structure comprised of five Cu(II) centers, {[Cu$_2$(Hsersal)$_2$(H$_2$O)]·H$_2$O}$_n$, (1), {[Cu$_2$(Hser-5OMe-sal)$_2$(H$_2$O)]·DMF}$_n$ (2), {[Cu$_2$(Hser-5NO$_2$-sal)$_2$(H$_2$O)]·2H$_2$O}$_n$ (3), {[Cu$_2$(Hser-5Cl-sal)$_2$(H$_2$O)]·2H$_2$O}$_n$ (4), {[Cu$_2$(Hser-3Cl-sal)$_2$(H$_2$O)]·3H$_2$O}$_n$ (5) and {[Cu$_2$(Hser-o-Van)$_2$(H$_2$O)]·3H$_2$O}$_n$ (6) and their conversion to the corresponding SCCs, [Cu$_2$(4,4'-bpy)(Hsersal)$_2$]·2H$_2$O (7), [Cu$_2$(4,4'-bpy)(Hser-5-OMe-

sal)$_2$]·6H$_2$O (8), [Cu$_2$(4,4'-bpy)(Hser-5-NO$_2$-sal)$_2$]·H$_2$O (9) and [Cu$_2$(4,4'-bpy)(Hser-5-Cl-sal)$_2$]·4H$_2$O·DMF (10), respectively (where H$_3$sersal = N-(2-hydroxybenzyl)-serine, H$_3$ser-5OMe-sal = N-(2-hydroxy-5-methoxybenzyl)-serine, H$_3$ser-5NO$_2$-sal = N-(2-hydroxy-5-nitrobenzyl)-serine, H$_3$ser-5-Cl-sal = N-(2-hydroxy-5-chlorobenzyl)-serine, H$_3$ser-3-Cl-sal = N-(2-hydroxy-3-chlorobenzyl)-serine, H$_3$ser-o-van = N-(2-hydroxy-3-methoxybenzyl)-serine and 4,4'-bpy = 4,4'-bipyridine). Figure 1 shows the structures of the ligands. In addition to their complete structural characterization by various analytical techniques including variable temperature magnetic susceptibility measurements, as an example water adsorption studies of **1** and **7** were carried out to demonstrate the change in the porous nature of the SCCs compared to the CPs.
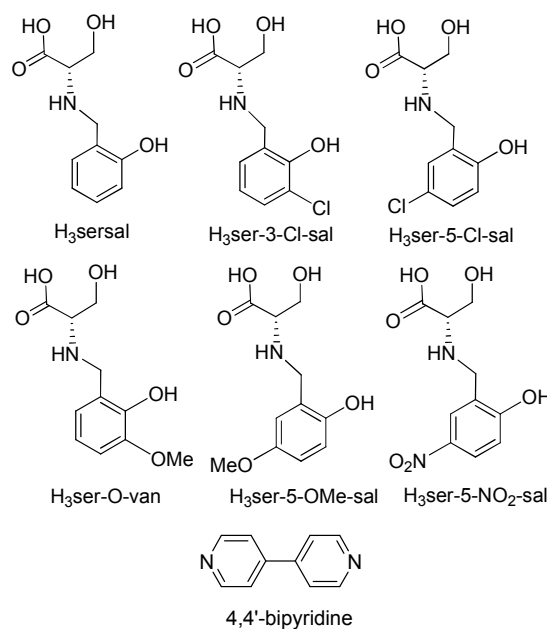
Fig. 1 Structure of the chiral ligands and neutral linker used in this study.

Experimental section

Materials and methods. All chemicals and solvents used for synthesis were obtained from commercial sources and were used as received, without further purification. All reactions were carried out under aerobic conditions. The H$_3$sersal ligand was prepared using a modified literature procedure.[21]

Physical measurements. ^{1}H NMR spectra of the sodium salt of the ligands were obtained in D$_2$O at 25 °C on a Bruker ARX-400 spectrometer; chemical shifts are reported relative to the residual solvent signals. The elemental analysis (C, H, N) was carried out using a Thermo Scientific CHNS analyzer; thermogravimetric analysis was carried out from 25 to 500 °C (at a heating rate of 10 °C/min) under dinitrogen atmosphere on Shimadzu DTG-60. IR spectra were measured in the 4000-400 cm^{-1} range on a Perkin-Elmer Spectrum I spectrometer with samples prepared as KBr pellets. UV-Vis spectra of the compounds in methanol (a typical concentration of 1 mM) were recorded in a Cary 60 UV-Vis spectrophotometer by Agilent

Technologies using a quartz cuvette of path length 10 mm. ESI mass spectrometry was performed using either Waters HRMS instrument or Thermo Scientific LTQ XL LC-MS instrument for the 50-2000 amu range. Raman spectra were recorded on a Renishaw InVia Raman microscope equipped with a 785 nm high-power near-infrared laser working at 300 mW power and a Renishaw CCD detector. Analysis of the Raman spectra were performed in reflection mode on powder samples placed on the sample stage and aligned in optical path by using a camera, with 0.1-0.5% laser power and by using 50X optics in the range of 400-2000 cm^{-1}. Optical rotations were recorded using an Anton Paar modular circular Polarimeter (MCP 300) using a glass cell with a 50 mm path length. CD spectra were recorded on a Chirascan spectropolarimeter (Applied Photophysics, Leatherhead, Surrey, UK) using quartz cuvettes with a 2 mm path length. Magnetic susceptibility measurements were carried out using the VSM option of an EC-II PPMS Quantum Design system to obtain χ versus temperature T in the temperature range 2 K to 380 K in an applied magnetic field H = 1 T, and the magnetization M versus magnetic field H at T = 2 K.

Synthesis of H₃sersal. To a solution of 500 mg of L-serine (4.8 mmol) and 190 mg of NaOH (4.8 mmoles) in 20 mL of a methanol:water mixture (v/v 1:1) was added 0.5 mL (4.8 mmol) of salicylaldehyde. The resulting yellow solution was stirred for an hour at room temperature. 181 mg of $NaBH_4$ (4.8 mmol) was added to it at 0 °C and the solution was stirred until the yellow color disappeared. The pH of the solution was adjusted to 5 using (~2 mL) glacial acetic acid and stirred for half an hour. A white precipitate thus formed was filtered off, washed with methanol and air dried. Yield: 0.824 g (82%). MS (ESI-TOF): m/z calcd for $[(H_3sersal)H]^+$, 212.0923; found, 212.0939. Anal. Calc. for $H_3sersal·0.5H_2O$ ($C_{10}H_{14}NO_{4.5}$, MW 220.09): Calc. C, 55.02; H, 6.41; N, 6.36. Found: C, 55.11; H, 5.93; N, 6.29. Mpt. 205 °C. ^1H NMR (D_2O): δ 3.21 (t, 1H), 3.69- 3.72 (m, 2H), 3.80 (q, 2H), 6.56–6.60 (m, 2H), 7.00–7.06 (m, 2H). Selected FTIR peaks (KBr, cm^{-1}): 3245(br), 3197(s), 3063(s), 1625(s), 1596(s), 1534(s), 1471(s), 1455(w), 1276(s), 1201(s), 1080(s), 758, 648. Specific rotation $_D[\alpha]^{20}$ = -24.24 (0.033%, CH_3OH). UV-Vis [λ, nm]: 205, 275.

Synthesis of H₃ser-5-methoxy-sal. It was prepared following the procedure described for H₃sersal except 0.594 mL (4.8 mmol) of 5-methoxysalicylaldehyde was used instead of salicylaldehyde. In this case, the resulting yellow Schiff base solution was stirred for 3h. Yield: 0.870 g (76%). MS (ESI-TOF): m/z calcd for $[(H_3ser-5-methoxy-sal)H]^+$, 242.1028; found, 242.1003. Anal. Calc. for $H_3ser-5-methoxy-sal·0.5H_2O$ ($C_{11}H_{16}NO_{5.5}$, MW 250.10): Calc. C, 52.28; H, 6.44; N, 5.60. Found: C, 52.29; H, 6.27; N, 5.44. M.pt. 211 °C. ^1H NMR (D_2O): δ 3.11 (t, 1H), 3.43-3.55 (q, 2H), 3.56-3.59 (m, 1H), 3.60 (s, 3H), 3.64- 3.68(m, 1H), 6.42 (d, 1H) 6.58-6.61 (q, 1H), 6.70 (d, 1H). Selected FTIR (KBr, cm^{-1}): 3245(br), 3180(w), 2833(s), 1631(s), 1598(w), 1568(w), 1516(s), 1455(w), 1362(w), 1322(m), 1267(s), 1230(s), 1077(s), 988(s), 809(s).

Synthesis of H₃ser-5NO₂-sal. It was prepared following the procedure described for H₃sersal except 795 mg (4.8 mmol) of 5-nitro salicylaldehyde was used instead of salicylaldehyde. Yield: 1 g (82%). MS (ESI-TOF): m/z calcd for $[(H_3ser-5NO_2-sal)H]^+$, 257.0774; found, 257.0797. Anal. Calc. for $H_3ser-5NO_2-sal·3H_2O$ ($C_{10}H_{18}N_2O_9$, MW 310.10): Calc. C, 38.69; H, 4.85; N, 9.03. Found: C, 39.19; H, 4.62; N, 8.62. M.pt. 204 °C. ^1H NMR (D_2O): δ 3.09 (t, 1H), 3.39-3.53 (q, 2H), 3.54-3.65 (m, 2H), 6.34 (d, 1H) 7.83-7.86 (q, 1H), 7.92 (d, 1H). Selected FTIR (KBr, cm^{-1}): 3608(s), 3301(br), 1639(br), 1586(m), 1531(m), 1492(s), 1446(w), 1339(s), 1296(s), 1137(s), 1102(s), 1086(s), 837(s), 754(s).

Synthesis of H₃ser-5-Cl-sal. It was prepared following the procedure described for H₃sersal except 745 mg (4.8 mmol) of 5-chlorosalicylaldehyde was used instead of salicylaldehyde. In this case, the resulting yellow Schiff base solution was stirred for 3h. Yield: 0.550 g (47%). MS (ESI-TOF): m/z calcd for $[(H_3ser-5-Cl-sal)H]^+$, 246.0533; found, 246.0500. Anal. Calc. for $H_3ser-5-Cl-sal$ ($C_{10}H_{12}NO_4Cl$, MW 245.53): Calc. C, 48.87; H, 4.93; N, 5.70. Found: C, 48.93; H, 4.81; N, 5.61. M.pt. 214 °C. ^1H NMR (D_2O): δ 3.11 (t, 1H), 3.43-3.55 (q, 2H), 3.56-3.59 (m, 1H), 3.60 (s, 3H), 3.64-3.68 (m, 1H), 6.42 (d, 1H) 6.58-6.61 (q, 1H), 6.70 (d, 1H). Selected FTIR peaks (KBr, cm^{-1}): 3257(br), 3196(s), 3063(s), 1629(s), 1592(s), 1535(s), 1477(m), 1446(m), 1362(s), 1272(s), 1199(s), 1078(s), 987(s), 824(s), 661(s).

Synthesis of H₃ser-3-Cl-sal. It was prepared following the procedure described for H₂sersal except 745 mg (4.8 mmol) of 3-chlorosalicylaldehyde was used instead of salicylaldehyde. In this case, the resulting yellow Schiff base solution was stirred for 3h. Yield: 0.440 g (40%). MS (ESI-TOF): m/z calcd for $[(H_3ser-3-Cl-sal)H]^+$, 246.0533; found, 246.0482. Anal. Calc. for $H_3ser-3-Cl-sal$ ($C_{10}H_{12}NO_4Cl$, MW 245.53): Calc. C, 48.87; H, 4.93; N, 5.70. Found: C, 48.91; H, 4.83; N, 5.59. M.pt. 203 °C. ^1H NMR (D_2O): δ 3.11 (t, 1H), 3.46 (d, 1H), 3.55-3.59 (m, 2H), 3.64-3.68 (m, 1H), 6.33 (t, 1H), 6.92 (d, 1H), 7.07 (d, 1H). Selected FTIR (KBr, cm^{-1}): 3138(br), 3020(w), 2851(m), 1640(s), 1597(s), 1511(s), 1461(s), 1437(s), 1388(s), 1359(s), 1320(s), 1249(s), 1227(s), 1071(s), 938(s), 771(s).

Synthesis of H₃ser-o-van. It was prepared following the procedure described for H₃sersal except 723 mg (4.8 mmol) of o-vanillin was used instead of salicylaldehyde. In this case, the resulting yellow Schiff base solution was stirred for 3h. Yield: 0.630 g (55%). MS (ESI-TOF): m/z calcd for $[(H_3ser-o-van)H]^+$, 242.1028; found, 242.1029. Anal. Calc. for $H_3ser-o-van·0.5H_2O$ ($C_{11}H_{16}NO_{5.5}$, MW 250.10): Calc. C, 52.78; H, 6.44; N, 5.60. Found: C, 52.58; H, 6.14; N, 5.85. M.pt. 215 °C. ^1H NMR (D_2O): δ 3.11 (t, 1H), 3.41-3.57 (m, 3H), 3.59 (s, 3H), 3.63- 3.68 (m, 1H), 6.35 (t, 1H) 6.67-6.71 (m, 2H). Selected FTIR (KBr, cm^{-1}): 3151(br), 3047(w), 2839(s), 1636(s), 1596(s), 1493(m), 1462(s), 1438(s), 1386(s), 1366(w), 1273(s), 1185(s), 1093(s), 948(s), 735(s).

Synthesis of {[Cu₂(Hsersal)₂(H₂O)]˙2.5H₂O}ₙ (1). In a 10 mL round bottom flask, 59 mg (0.24 mmol) of CuSO₄.5H₂O was dissolved in 2 mL methanol. To this was added a clear solution of K₂Hsersal which was prepared by using 50 mg (0.24 mmol) of H₃sersal and 26 mg (0.48 mmol) of potassium hydroxide in 2 mL of methanol. The reaction mixture turned green and was stirred for 6 hrs at room temperature. The resulted green slurry was taken to dryness. Addition of 10 mL DMF to the solid followed by filtration provided a green filtrate which upon evaporation gave the desired product. The compound was recrystallized from methanol. Yield: 42 mg (65%). Anal. Calc. for $C_{20}H_{29}N_2O_{11.5}Cu_2$ (MW 608.52): Calc. C, 39.47; H, 4.76; N, 4.60. Found: C, 39.41; H, 4.61; N, 4.52. Selected FTIR peaks (KBr, cm^{-1}): 3400(br), 3233(s), 2937(s), 1613(s), 1581(s), 1486(s), 1449(s), 1253(s), 1116(w), 1043(s), 757. ESI-MS: [Cu₂(Hsersal)₂]H⁺, (m/z, calc. 546.51; found 545.69). UV-Vis [λmax, nm (ε, L·mol^{-1}·cm^{-1})]: 675 (123). Specific rotation $_D[\alpha]^{20}$ = +26.3 (0.023%, CH₃OH).

Synthesis of {[Cu₂(Hser-5OMe-sal)₂(H₂O)]˙DMF}ₙ (2). It was prepared following the procedure described for **1** except K₂Hser-5OMe-sal [50 mg (0.20 mmol) of H₃ser-5OMe-sal and 24 mg (0.40 mmol) of potassium hydroxide] was used instead of K₂Hsersal. Yield: 47 mg (75%). Anal. Calc. for $C_{25}H_{35}N_3O_{12}Cu_2$ (MW 696): Calc. C, 43.10; H, 5.02; N, 6.03. Found: C, 42.74; H, 4.99; N, 5.93. Selected FTIR peaks (KBr, cm^{-1}): 3400(br), 3239(w), 1633(s), 1603(s), 1492(s), 1456(w), 1390(s), 1350(m), 1268(s), 1222(s), 1156(s), 1090(m), 1042(s), 804(s), 718(s). UV-Vis [λmax, nm (ε, L·mol^{-1}·cm^{-1})]: 680 (48). Specific rotation $_D[\alpha]^{20}$ = +34.92 (0.006%, CH₃OH).

Synthesis of {[Cu₂(Hser-5NO₂-sal)₂(H₂O)]}ₙ (3). It was prepared following the procedure described for **1** except K₂Hser-5NO₂-sal [50 mg (0.20 mmol) of H₃ser-5NO₂-sal and 22 mg (0.40 mmol) of potassium hydroxide] was used instead of K₂Hsersal. Yield: 26 mg (40%). Anal. Calc. for $C_{20}H_{22}N_4O_{13}Cu_2$ (MW 653): Calc. C, 36.75; H, 3.36; N, 8.57. Found: C, 37.11; H, 3.68; N, 8.33. Selected FTIR peaks (KBr, cm^{-1}): 3430(br), 3225(s), 1627(s), 1601(s), 1481(s), 1340(s), 1303(s), 1188(s), 1100(s), 1025(s), 899(s), 658(s). UV-Vis [λmax, nm (ε, L·mol^{-1}·cm^{-1})]: 684 (70). Specific rotation $_D[\alpha]^{20}$ = +8.0 (0.012%, CH₃OH).

Synthesis of {[Cu₂(Hser-5Cl-sal)₂(H₂O)]˙2H₂O}ₙ (4). It was prepared following the procedure described for **1** except K₂Hser-5Cl-sal [50 mg (0.20 mmol) of H₃ser-5Cl-sal and 23 mg (0.40 mmol) of potassium hydroxide] was used instead of K₂Hsersal. Yield: 25 mg (40%). Anal. Calc. for $C_{20}H_{26}N_2O_{11}Cu_2$ (MW 668): Calc. C, 35.92; H, 3.89; N, 4.19. Found: C, 36.22; H, 3.70; N, 4.10. Selected FTIR peaks (KBr, cm^{-1}): 3371(br), 3234(br), 1622(br), 1477(s), 1418(m), 1385(w), 1352(w), 1267(s),1191(s), 1125(s), 1092(m), 874(s), 667(s). UV-Vis [λmax, nm (ε, L·mol^{-1}·cm^{-1})]: 663 (34). Specific rotation $_D[\alpha]^{20}$ = +32.97 (0.019%, CH₃OH).

Synthesis of {[Cu₂(Hser-3Cl-sal)₂(H₂O)]˙3H₂O}ₙ (5). It was prepared following the procedure described for **1** except K₂Hser-3Cl-sal [50 mg (0.20 mmol) of H₃ser-3Cl-sal and 23 mg (0.40 mmol) of potassium hydroxide] was used instead of K₂Hsersal. Yield: 42 mg (76%). Anal. Calc. for $C_{20}H_{28}N_2O_{12}Cu_2$ (MW 686): Calc. C, 34.98; H, 4.08; N, 4.08. Found: C, 34.98; H, 3.80; N, 4.02. Selected FTIR peaks (KBr, cm^{-1}): 3389(br), 3230(br), 1627(br), 1590(s), 1445(s), 1354(m), 1315(w), 1280(m), 1240(w), 1176(s), 1137(s), 1092(m), 846(s), 744(s). UV-Vis [λmax, nm (ε, L·mol^{-1}·cm^{-1})]: 679 (64). Specific rotation $_D[\alpha]^{20}$ = -18.08 (0.019%, CH₃OH).

Synthesis of {[Cu₂(Hser-o-Van)₂(H₂O)]˙3H₂O}ₙ (6). It was prepared following the procedure described for **1** except K₂Hser-o-Van [50 mg (0.20 mmol) of H₃ser-o-Van and 24 mg (0.40 mmol) of potassium hydroxide] was used instead of K₂Hsersal. Yield: 30 mg (48%). Anal. Calc. for $C_{22}H_{34}N_2O_{14}Cu_2$ (MW 677.5): Calc. C, 38.90; H, 5.06; N, 4.17. Found: C, 39.12; H, 4.55; N, 4.04. Selected FTIR peaks (KBr, cm^{-1}): Selected FTIR (KBr, cm^{-1}): 3401(br), 3226(w), 1633(br), 1478(s), 1384(w), 1354(m), 1267(m), 1237(s), 1186(w), 1079(s), 847(s), 740(s). UV-Vis [λmax, nm (ε, L·mol^{-1}·cm^{-1})]: 672 (55). Specific rotation $_D[\alpha]^{20}$ = +17.6 (0.012%, CH₃OH).

Synthesis of [Cu₂(4,4'-bpy)(Hsersal)₂]˙2H₂O (7). In a 10 mL round bottom flask, 25 mg (0.04mmol) of **1** was dissolved in 3 mL methanol. To this was added 6 mg (0.04 mmol) of 4,4'-bipyridine and the mixture was stirred for 6 hours under reflux conditions. The green solution was evaporated completely to isolate **7**. Yield: 21 mg (69%). It can also be directly prepared by refluxing a methanolic solution of CuSO₄·5H₂O, K₂Hsersal and 4,4'-bipyridine in a 1:1:0.5 ratio for 6 hours with an yield of 64%. Anal. Calcd. For $C_{30}H_{34}N_4O_{10}Cu_2$ (MW 737.69): Calc. C, 48.84; H,4.61; N, 7.59. Found: C, 49.07; H, 4.73; N, 8.05. Selected FTIR peaks (KBr, cm^{-1}): 3355(br), 3196(s), 2924(s), 1616(s), 1596(s), 1534(w), 1479(s), 1455(s), 1276(br), 1217(s), 1092(s), 758(s), 644(s). ESI-MS: [Cu₂(Hsersal)₂ (4,4'bipyridine)]H⁺, (m/z, calc. 702.69; found 702.82), [Cu₂(Hsersal)₂]H⁺ (m/z, calc. 546.51; found 545.04). UV-Vis [λmax, nm (ε, L·mol^{-1}·cm^{-1})]: 655 (213). Specific rotation, $_D[\alpha]^{20}$ = +50.60 (0.02%, CH₃OH).

Synthesis of [Cu₂(4,4'-bpy)(Hser-5-OMe-sal)₂]˙6H₂O (8). It was prepared following the procedure described for **7** except **2** was used instead of **1**. Yield: 28 mg (71%). Anal. Calc. for $C_{32}H_{46}N_4O_{16}Cu_2$ (MW 869): Calc. C, 44.18; H, 5.29; N, 6.44. Found: C, 43.70; H, 4.71; N, 5.87. Selected FTIR peaks (KBr, cm^{-1}): Selected FTIR (KBr, cm^{-1}): 3479(br), 3270(w), 3157 (m), 1657(m), 1606(s), 1495(s), 1424 (m), 1348(m), 1231(m), 1217(s), 1098(w), 1026(s), 802(s), 674(w). UV-Vis [λmax, nm (ε, L·mol^{-1}·cm^{-1})]: 657 (40). Specific rotation $_D[\alpha]^{20}$ = +91.20 (0.012%, CH₃OH).

Synthesis of [Cu₂(4,4'-bpy)(Hser-5-NO₂-sal)₂]˙H₂O (9). It was prepared following the procedure described for **7** except **3** was used instead of **1**. However, in this case, the product was

totally insoluble in methanol and isolated via filtration and air-dried. Yield: 24 mg (60%). Anal. Calc. for $C_{30}H_{30}N_6O_{13}Cu_2$ (MW 809): Calc. C, 44.49; H, 3.70; N, 10.38. Found: C, 44.11; H, 3.14; N, 10.07. Selected FTIR peaks (KBr, cm⁻¹): Selected FTIR (KBr, cm⁻¹): 3410(br), 3229(m), 1642(s), 1597(s), 1477(s), 1439(w), 1394(w), 1353(m), 1290(br), 1217(s), 1185(m), 1079(s), 936(s), 645(s). UV-Vis [λmax, nm (ε, L·mol⁻¹·cm⁻¹)]: 680 (21). Specific rotation $_D[\alpha]^{20}$ = -16.0 (0.012%, CH_3OH).

Synthesis of [Cu₂(4,4'-bpy)(Hser-5-Cl-sal)₂]·4H₂O·DMF (10). It was prepared following the procedure described for **7** except **4** was used instead of **1**. Yield: 26 mg (67%). Anal. Calc. for $C_{33}H_{43}N_5O_{13}Cu_2$ (MW 915): Calc. C, 43.52; H, 4.37; N, 7.56. Found: C, 43.27; H, 4.69; N, 7.65. Selected FTIR peaks (KBr, cm⁻¹): Selected FTIR (KBr, cm⁻¹): 3382(br), 3235(w), 1634(s), 1614(s), 1473(s), 1417(s), 1389(w), 1350(m), 1287(s), 1219(s), 1123(w), 1070(s), 821(s), 644(s). UV-Vis [λmax, nm (ε, L·mol⁻¹·cm⁻¹)]: 673 (40). Specific rotation $_D[\alpha]^{20}$ = +27.2 (0.012%, CH_3OH).

Single crystal X-ray structure determination. Following the general practices published earlier,[22] initial crystal evaluation and data collection were performed on a Kappa APEX II diffractometer equipped with a CCD detector (with the crystal-to-detector distance fixed at 60 mm) and sealed-tube monochromated MoKα radiation using the program APEX2.[23] By using the program SAINT[23] for the integration of the data, reflection profiles were fitted, and values of F^2 and $\sigma(F^2)$ for each reflection were obtained. A lot of efforts were invested to recollect data sets with new crystals a few times but no better data sets that are used here could be obtained. Data were also corrected for Lorentz and polarization effects. The subroutine XPREP[23] was used for the processing of data that included determination of space group, application of an absorption correction (SADABS)[23], merging of data, and generation of files necessary for solution and refinement. The crystal structures were solved and refined using SHELX 97.[24] In each case, the space group was chosen based on systematic absences and confirmed by the successful refinement of the structure. Furthermore, Flack parameters of all the structures confirmed the correct absolute configurations. Positions of most of the non-hydrogen atoms were obtained from a direct methods solution. Several full-matrix least-squares/difference Fourier cycles were performed, locating the remainder of the non-hydrogen atoms. In order to obtain reasonable thermal parameters compared to other atoms, the lowest residual factors and optimum goodness of fit with convergence of refinement, occupancy factors of some of the atoms were adjusted accordingly. The lattice water molecules (O5, O6 and O7) in **7** were adjusted to 0.5 and refined isotropically. In the final difference Fourier map of **7**, other than a peak of 1.31 e/Å³ located at 0.94 Å from O5, there was no other significant peaks >1 e/Å³. All hydrogen atoms except for water molecules in the asymmetric unit of 7 were placed in ideal positions and refined as riding atoms with individual isotropic displacement

parameters. The occupancy factor of the lattice methanol molecule (O7 and C16) in **8** was adjusted to 0.5. All hydrogen atoms except for the oxygen (O7) of the lattice methanol molecule in the asymmetric unit of **8** were placed in ideal positions and refined as riding atoms with individual isotropic displacement parameters. In the final difference Fourier map of **8**, other than a peak of 1.17 e/Å³ located at 0.75 Å from O7, there were no other significant peaks >1 e/Å³. The occupancy factors of all the atoms (C18, C19, O8 and S2) of one of the lattice DMSO molecule in **9** were adjusted to 0.5 and refined isotropically. In the final difference Fourier map of **9**, other than a peak of 1.10 e/Å³ located at 1.60 Å from O8, there was no other significant peaks >1 e/Å³. All hydrogen atoms except for the above DMSO molecule in the asymmetric unit of **9** were placed in ideal positions and refined as riding atoms with individual isotropic displacement parameters. All non-hydrogen atoms for all structures were refined with anisotropic displacement parameters except where mentioned. Crystallographic parameters and basic information pertaining to data collection and structure refinement for **1**, **4**, **7**, **8** and **9** are summarized in Table 1. All figures were drawn using MERCURY V 3.0[25] and hydrogen bonding parameters were generated using PLATON.[26] The final positional and thermal parameters of the non-hydrogen atoms for all structures are listed in the CIF files (ESI†).

Powder X-ray studies. Data were recorded on a Rigaku Ultima IV diffractometer equipped with a 3 KW sealed tube Cu Kα X-ray radiation (generator power settings: 40 kV and 40 mA) and a DTex Ultra detector using parallel beam geometry (2.5° primary and secondary solar slits, 0.5° divergence slit with 10 mm height limit slit). Each sample grounded into a fine powder using a mortar and a pestle was placed on a glass sample holder that was placed on the sample rotation stage (120 rpm) attachment. The data were collected over an angle range 5° to 50° with a scanning speed of 1° per minute with 0.02° step with XRF reduction for the metals.

Water adsorption measurements. Data were recorded for pressures in the range 0–1.2 bar by the volumetric method using a BELSORP instrument. Each solid sample was transferred to pre-weighed analysis tubes, which were capped with transeals and evacuated by heating at a temperature between 110-150 °C (based on thermal profile obtained from TGA) under dynamic vacuum until an outgas rate of less than 2 mTorr min-1 (0.27 Pa min⁻¹) was achieved (ca. 12-24 hrs). The evacuated analysis tubes containing the degassed sample was then carefully transferred to an electronic balance and weighed again to determine the mass of sample. The tube was then placed back on the analysis port of the gas adsorption instrument. The outgas rate was again confirmed to be less than 2 mTorr min⁻¹ (0.27 Pa min⁻¹). For all isotherms, warm and cold free-space (dead volume) correction measurements were performed using ultra-high-purity He gas (UHP grade 5.0, 99.999% purity). The change of the pressure was monitored and the degree of adsorption was determined by the decrease in

pressure at the equilibrium state via computer controlled automatic operations that are set up at the start of each measurement. Oil-free vacuum pumps and oil-free pressure regulators were used for all measurements to prevent contamination of the samples during the evacuation process or of the feed gases during the isotherm measurements.

Results and discussion

Synthesis. The synthesis of the H_3sersal ligand was done with slight modification from the literature procedure. A detailed characterization by several methods not only established its purity but also was helpful in comparing with its metal complexes. Compounds **1-6** were obtained by stirring a methanolic solution of $CuSO_4 \cdot 5H_2O$ and the respective ligand (in a 1:1 ratio) for 6 hours at room temperature; the same products are obtained if the reactions are carried out under reflux conditions. This shows their stability towards heating in a solvent. Conversion of **1** to **7**, **2** to **8**, **3** to **9** and **4** to **10** was achieved by refluxing a methanolic solution of **1** or **2** or **3** or **4** and 4,4'-bipyridine for 6 hrs, respectively (see Scheme 1). Compounds **7-10** can also be directly prepared by refluxing a

methanolic solution of $CuSO_4 \cdot 5H_2O$, the respective ligand and 4,4'-bipyridine (in a 1:1:0.5 ratio). It should be noted here that the reaction of $Cu(CH_3COO)_2 \cdot 2H_2O$ with Li_2Hsersal under ambient conditions resulted in the formation of a trinuclear complex, $\{[Cu_3(Hsersal)_3(H_2O)_2] \cdot 2H_2O\}_n$ reported by Vittal et al.[21]

Single crystal structure analyses. Crystals of **1**, **4**, **7** and **8** suitable for the single crystal X-ray study were grown from slow evaporation of the respective methanolic solution: **1** in 8-10 days, **2** in 15 days, **7** in one day and **8** in 3-4 days. Crystals of **9** were grown from slow evaporation of a DMSO:methanol (1:1) solution in 20 days.

Compounds **1** and **4** are isostructural but **1** crystallizes in the orthorhombic chiral space group $P2_12_12_1$ and **4** crystallizes in the monoclinic chiral space group $P2_1$. The dimeric subunit of both **1** and **4** (shown in Fig. S1 and S2, ESI) consists of two copper(II) centers and two Hsersal ligands. The asymmetric unit of **1** contains one lattice water molecule while that of **4** contains one methanol molecule. The two Cu(II) centers in the subunit are not equivalent. In the dimeric unit, one

For **1**: X = H, Y= H;   For **2**: X = H, Y= OMe
For **3**: X = H, Y= NO$_2$;   For **4**: X = H, Y= Cl
For **5**: X = Cl, Y= H;   For **6**: X = OMe, Y= H

For **7**: X = H, Y= H;   For **8**: X = H, Y= OMe
For **9**: X = H, Y= NO$_2$;   For **10**: X = H, Y= Cl

Crystal structures of **1**, **4**, **7**, **8** and **9** are reported.
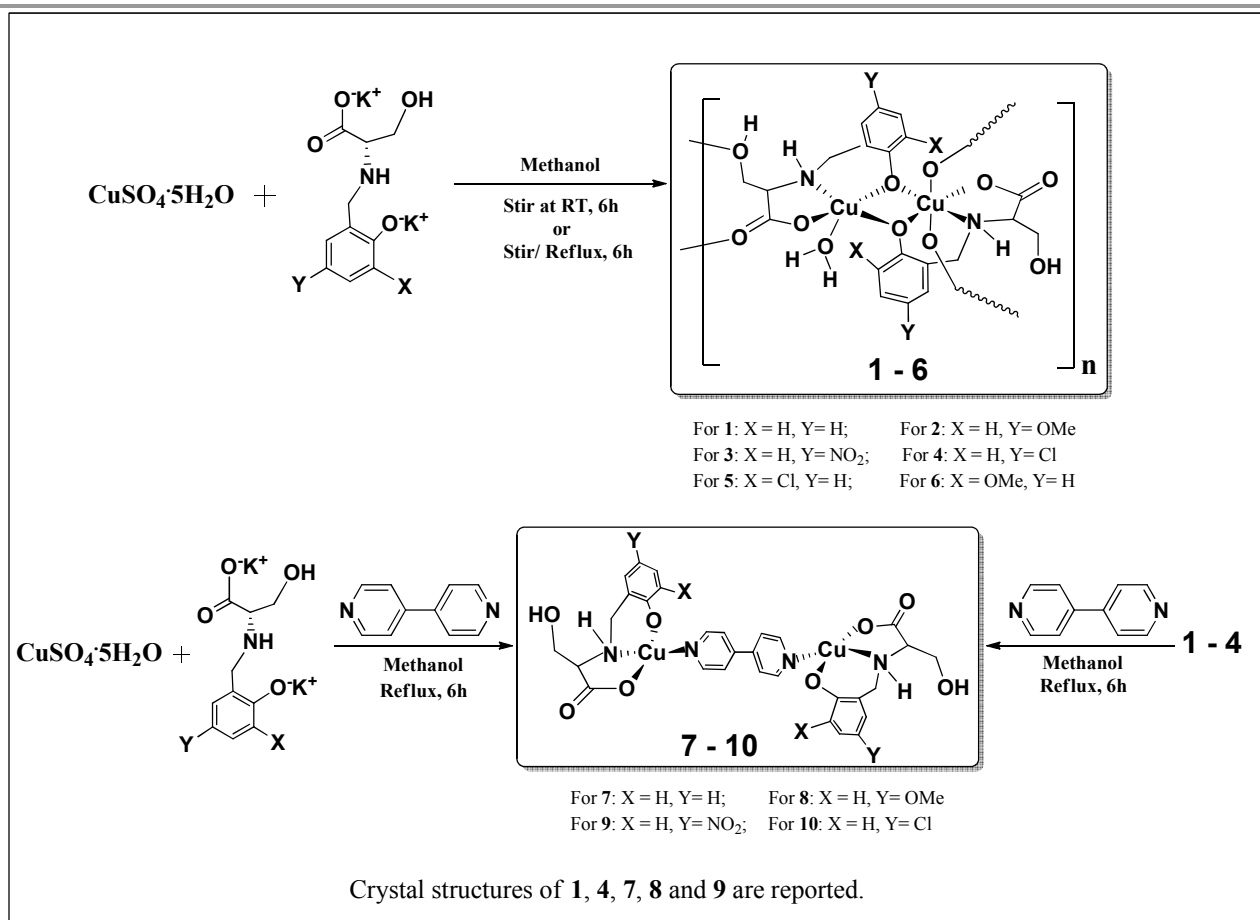
Scheme 1 General scheme for the synthesis of **1-6** and **7-10**.

Journal Name

ARTICLE

Table 1 Crystal structure data and refinement parameters for **1**, **4**, **7**, **8** and **9**.

Compound	1	4	7	8	9
Chemical Formula	$C_{20}H_{26}Cu_2N_2O_{10}$	$C_{24}H_{27}Cl_2Cu_2N_4O_6$	$C_{21}H_{26}Cu_2N_2O_{10}Cl_2$	$C_{33}H_{38}Cu_2N_4O_{11}$	$C_{36}H_{46}Cu_2N_6O_{15}S_3$
Formula Weight	581.51	665.47	664.44	793.75	1026
Temperature (K)	150(2)	180(2)	150(2)	180(2)	180(2)
Wavelength (Å)	0.71073	0.71073	0.71073	0.71073	0.71073
Crystal System	Orthorhombic	Monoclinic	Monoclinic	Monoclinic	Monoclinic
Space Group	$P2_12_12_1$	$P2_1$	$C2$	$C2$	$C2$
a (Å)	7.4080(10)	7.4056(15)	25.187(5)	24.808(6)	23.4909(19)
b (Å)	14.011(2)	13.343(3)	6.6672(13)	6.1829(13)	6.8770(5)
c (Å)	21.402(4)	13.433(3)	10.488(2)	10.517(3)	13.6838(12)
a (°)	90	90	90	90	90
β (°)	90	103.786(3)	100.653(11)	100.984(4)	101.667(5)
g (°)	90	90	90	90	90
Z	4	2	2	2	2
V (Å^3)	2221.4(6)	1289.1(5)	1730.9(6)	1745.0(7)	2164.9(3)
Density (mg/cm^3)	1.709	1.714	1.415	0.986	1.781
μ(mm^{-1})	1.971	1.906	1.286	0.656	2.104
F(000)	1160	678	760	542	1140
Theta (°) Range for Data Coll.	1.74° to 25.04°	2.18° to 24.99°	1.98° to 25.04°	1.67° to 25.16°	1.77° to 25.06°
Reflections Collected	14127	9580	5622	8112	7839
Independent Reflections	3915	4231	3007	2287	3380
Reflections with I >2σ(I)	3314	4086	2804	2115	2723
R_{int}	0.0567	0.0186	0.0168	0.0268	0.0431
No. of Parameters refined	305	344	208	228	281
GOF on F^2	0.967	1.177	1.091	1.098	0.935
Final R_1^a/wR_2^b (I >2σ(I))	0.0415/0.0882	0.0195/ 0.0421	0.0524/0.1632	0.0490/0.1434	0.0494/0.1315
R_1/wR_2 (all data)	0.0561/0.0954	0.0205/0.0423	0.0558/0.1657	0.0534/.1518	0.0654/0.1451
Flack Parameter	0.0(0)	0.0(0)	0.0(0)	0.0(0)	0.0(0)
Largest diff. peak and hole (eÅ^{-3})	1.002 and -0.592	0.235 and -0.231	1.311 and -0.479	1.169 and -0.391	1.099 and -0.405

$^aR_1 = \Sigma||F_o| - |F_c||/\Sigma|F_o|$. $^b wR_2 = [\Sigma w(F_o^2 - F_c^2)^2/\Sigma w(F_o^2)^2]^{1/2}$, where $w = 1/[\sigma^2(F_o^2) + (aP)^2 + bP]$, $P = (F_o^2 + 2F_c^2)/3$.

hexacoordinated Cu(II) is in distorted octahedral geometry (Cu1) and the other five coordinated Cu(II) is in distorted square pyramidal geometry (Cu2). The coordination environment around Cu1 is O$_5$N type; two sites are occupied by two bridging phenoxo oxygen, the third site is occupied by an oxygen atom of the carboxylate of Hsersal ligand for **1** and Hser-5-Cl-sal ligand for **4** binding in a monodentate fashion,

the fourth site is occupied by the N atom of ligand, the fifth site is occupied by oxygen of the bridging carboxylate of another ligand and the sixth site is occupied by the oxygen of hydroxyl group of the sidearm (CH$_2$OH) of another ligand. The coordination environment around Cu2 is O$_4$N type, where again as in Cu1 two sites are occupied by two bridging phenoxo oxygen, third site occupied by the oxygen of the monodentate

carboxylate of the ligand, the fourth site is occupied by the nitrogen of the amine group of the ligand but the fifth site is occupied by the oxygen atom (O8 in **1** and O9 in **4**) of the coordinated water molecule. Thus Cu1 is coordinating to five oxygens from four different ligands whereas Cu2 is coordinating to four oxygen atoms, three of which are from two ligands and one from the coordinated water molecule. The Cu...Cu distances in **1** and **4** are 3.002 Å and 2.997 Å, respectively, which fall in the range (2.950 Å - 3.023 Å) reported for compounds with the bis(phenoxo)dicopper core containing similar ligands.[15,16,18-22] Other bond distances (Cu-O$_{phenoxo}$, Cu-O$_{carboxy}$ and Cu-N$_{amine}$) in **1** and **4** are also found to be similar to those in these compounds.[16,18-21] The selected bond distances and bond angles for **1** and **4** are listed in Tables S1 and S2 of the ESI†. In both **1** and **4**, the carboxylate groups of the two ligands coordinating to the two copper centers show different binding modes: the carboxylate surrounding the Cu1 binds in a monodentate fashion with the uncoordinated oxygen atom O5 hydrogen bonded to the -CH$_2$OH group of another ligand but the carboxylate group coordinating to Cu2 is bridging between Cu2 of one asymmetric unit and Cu1 of next asymmetric unit. The two Cu--O$_{carb}$ bond distances are similar (1.937(5) Å and 1.942(6) Å for **1** and 1.925 (5) Å and 1.939 (6) Å for **4**). This connectivity of the ligands in **1** and **4** generates the 2D network shown in Fig. 2 and Fig. 4, respectively.

Within the 2D network in **1** and **4**, five copper centers (marked yellow in Fig. 3 for **1** and Fig. 5 for **4**) form a loop like structure that is repeated in both x and y directions. The dimension of the loop is 9.313 Å x 7.408 Å in **1** and 9.626 Å x 7.406 Å in **4**. This loop due to the diverse binding of the ligands is a unique structural feature in **1** and **4**.

Compared to the structures of **1** and **4**, in the trinuclear compound, {[Cu$_3$(Hsersal)$_3$(H$_2$O)$_2$]·2H$_2$O}$_n$, mentioned earlier[21] the asymmetric unit contains two Cu(II) centers connected by a bis(μ-phenoxo) bridge and the third Cu(II) center without a phenoxo-bridge. However, in all three compounds **1**, **4** and the trinuclear compound one of the two bis(μ-phenoxo) bridged Cu(II) is pentacoordinated while the other Cu(II) is hexacoordinated despite the fact that both carboxylates coordinating to Cu(II) in the trinuclear compound are bridging type compared to one monodendate carboxylate and one bridging carboxylate

in both **1** and **4**. This is due to the presence of two coordinated water molecules in the trinuclear compound whereas in **1** and **4** the pentacoordinated Cu(II) is coordinated to one water molecule. Even when a solvent molecule (water) is coordinating to one of the metal centers in the CPs, a 2D coordination polymer is formed through the coordination of the oxygen atom of the side arm CH$_2$OH of the ligand; such binding of an alcoholic group to a metal center like Cu(II) is not so common.
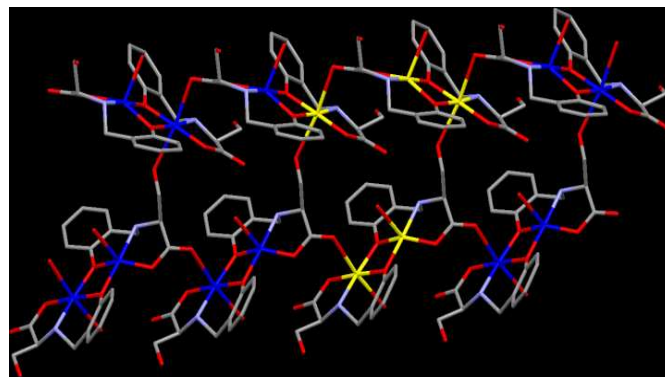
Fig. 3 A perspective view of the five Cu(II) atoms (yellow colored) forming a loop in **1**.

In **1** the water molecule (O8) coordinated to the Cu(II) is intermolecularly hydrogen bonded to the coordinated oxygen atom of the bridged carboxylate (O1) of the ligand (O---O distance: 2.80 Å) and also to the uncoordinated oxygen atom of the monodentate carboxylate (O5) of the ligand (O---O distance: 2.85 Å). The uncoordinated oxygen atom of the monodendate carboxylate (O5) is strongly hydrogen bonded to the oxygen atom (O7) of the –CH$_2$OH (O---O distance: 2.776 Å) of the ligand of the next asymmetric unit. The oxygen atom (O9) of the –CH$_2$OH of the ligand is strongly hydrogen bonded to the oxygen atom (O10) of the lattice water molecule (O---O distance: 2.679 Å). One of the nitrogen atoms (N2) shows intermolecular hydrogen bonding with the oxygen atom (O2) of bridged carboxylate (N-H---O distance: 3.254 Å) whereas the
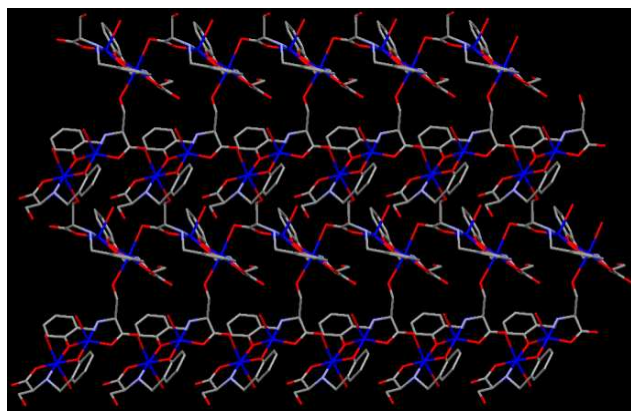
Fig. 2 A perspective view of the 2D coordination network in **1**.
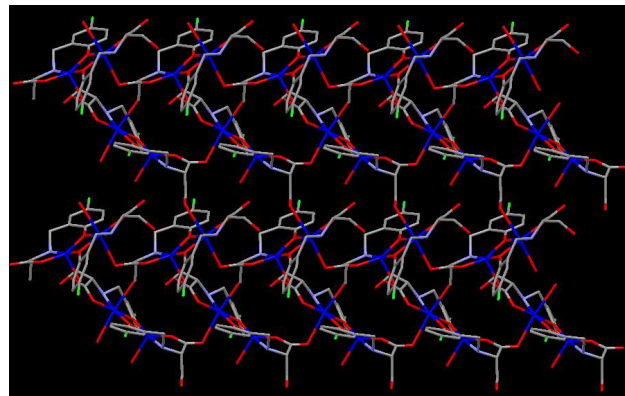
Fig. 4 A perspective view of the 2D coordination network in **4**.
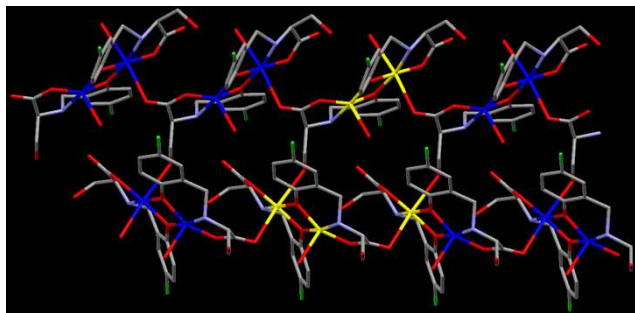
Fig. 5 A perspective view of the five Cu(II) atoms (yellow colored) forming a loop in **4**.

other nitrogen atom (N1) is hydrogen bonded intermolecularly to the oxygen atom (O5) of the monodentate carboxylate of the ligand (N-H---O distance: 3.087 Å).

Similarly, in **4** the corresponding coordinated water molecule (O9) is intermolecularly hydrogen bonded to both the coordinated oxygen atom of the bridged carboxylate (O5) (O---O distance: 2.83 Å) and the uncoordinated oxygen atom of the monodentate carboxylate (O2) of the ligand (O---O distance: 2.86 Å). The uncoordinated oxygen atom of the monodendate carboxylate (O2) is hydrogen bonded to oxygen atom (O8) of the –CH_2OH (O---O distance: 2.92 Å) of the ligand from the next asymmetric unit. The oxygen atom (O7) of the –CH_2OH of the ligand is also hydrogen bonded to the oxygen atom (O10) of the lattice methanol molecule (O---O distance: 2.87 Å). One of the nitrogen atoms (N1) is intermolecularly hydrogen bonded with the oxygen atom (O10) of lattice methanol molecule (N-H---O distance: 2.88 Å) whereas the other nitrogen atom (N2) is hydrogen bonded in an intermolecular fashion to the oxygen atom (O2) of the monodentate carboxylate of the ligand (N-H---O distance: 2.91 Å). The hydrogen bonding parameters for **1** and **4** are summarized in Table 2.

Compounds **7** and **8** are isostructural and crystallize in the monoclinic chiral *C*2 space group. In each case, there are two equivalent tetracoordinated copper centers with slightly distorted square planar geometry (as shown in Figs. S3 and S4, ESI). The coordination environment around each copper center in **7** and **8** is N_2O_2 type. One of the oxygen binding to Cu(II) is from the phenoxy group of the respective ligands and other from the carboxylate of the ligand whereas one nitrogen coordinating to the Cu(II) comes from the NH group of the ligand and the other from the 4,4'-bipyridine. The Cu-$O_{phenoxo}$, Cu-$O_{carboxy}$ and Cu-N_{amine} bond distances in **7** and **8** are similar to those found in **1** and **4** and other complexes mentioned above. The selected bond distances and bond angles for **7** and **8** in **7** and **8** is N_2O_2 type. One of the oxygen binding to Cu(II) is from the phenoxy group of the respective ligands and other from the carboxylate of the ligand whereas one nitrogen coordinating to the Cu(II) comes from the NH group of the ligand and the other from the 4,4'-bipyridine. The Cu-$O_{phenoxo}$, Cu-$O_{carboxy}$ and Cu-N_{amine} bond distances in **7** and **8** are similar to those found in **1** and **4** and other complexes mentioned

above. The selected bond distances and bond angles for **7** and **8** are listed in Tables S1 and S2 of the ESI. The asymmetric unit in **7** has two lattice water molecules whereas in **8** there is only one lattice methanol molecule. In each case, the 4,4'-bipyridine acts as a bridge between the two copper centers forming a discrete dinuclear unit. In **7** the two phenyl rings of 4,4'-bipyridine are arranged with a twist of -21.5° whereas in **8** these are arranged with a twist of -22.6°. In the literature such a twist of two pyridyl rings of 4,4'-bipyridine is also observed in [Cu_2(L-tryptophanato)$_2$(4,4'-bipyridine)(H_2O)$_2$](NO_3)$_2$, where the dihedral angles are 10.6° and 13.6°.[13] These are different from the polymeric coordination compounds reported in the literature with a general formula [Cu_2(L)$_2$(4,4'-bpy)]$_n$ where L can be any amino acid.[13,21,27-29] Furthermore, a compound with the formula [Cu(L')(4,4'-bpy)] is reported, where L' is the Schiff base form of the same ligand (H_3sersal) and 4,4'-bipyridine acts as a monodentate ligand.[30] Through intermolecular hydrogen bonding in **7**, the uncoordinated oxygen atom (O2) of the monodendate carboxylate connects oxygen atom (O4) of the CH_2OH (O---O distance: 2.68 Å) of the ligand of next asymmetric unit forming the supramolecular network of the [Cu_2(4,4'-bpy)(Hsersal)$_2$]·2H_2O (see Figs. 6a and 6b) with a pore size of 18.985 Å x 6.667 Å. The next layer of the discreet unit is also forming a hydrogen bonded 2D supramolecular assembly (see Fig. S5, ESI). These two 2D supramolecular assemblies are further joined via the solvent molecules (see Figs. S6a and S6b, ESI). The lattice water molecules sits inside
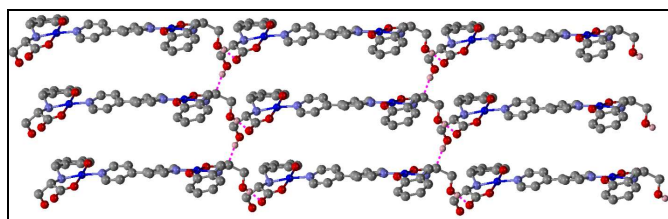
Fig. 6a Perspective view of the 2D supramolecular assembly in **7**.
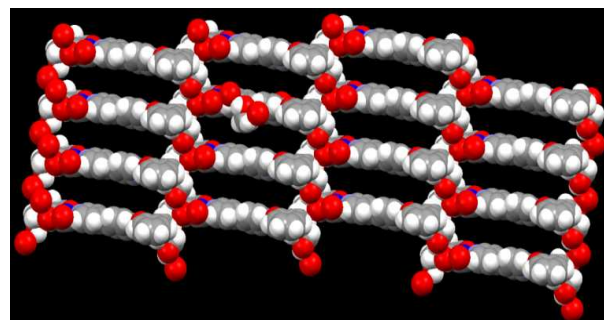
Fig. 6b Space fill representation of the supramolecular assembly in **7**.

the pores and are hydrogen bonded to each other (O6---O7 distance: 2.893 Å) as well as to the uncoordinated oxygen atom of the carboxylate of the ligand (O6---O2 distance: 2.922 Å). The 1st layer of supramolecular assembly overlaps with the 3rd and the 2nd layer overlaps with the 4th layer (see Fig. 7).

Table 2 Hydrogen Bonding Parameters for **1**, **4**, **7, 8** and **9**.

D–H…A	r (D-H) (Å)	r (H…A) (Å)	r (D…A) (Å)	∠D-H…A (deg)	Symmetry
1					
O7-H7...O5	0.868	1.98	2.776(6)	152	x-1, y, z
O8-H8B...O5	0.86	2.01	2.849(7)	166	-x+2, y+1/2, -z+1/2
O8-H8A...O1	0.86	2.02	2.800(7)	150	x+1, y, z
O9-H9...O10	0.82	1.88	2.679(13)	166	x+1/2, -y+3/2, -z
O10-H10A...O8	0.85	2.29	3.123(12)	164	
N1-H1…O5	0.98	2.13	3.087(8)	165	-x+2, y+1/2, -z+1/2
N2-H2...O2	0.98	2.64	3.254(7)	120	x+1, y, z
C2-H2A...O2	0.93	2.57	3.149(8)	121	
C7-H7A...O9	0.97	2.45	3.113(10)	125	
C12-H12...O4	0.93	2.37	3.159(9)	141	
C20-H20B...O4	0.97	2.6	3.281(8)	127	
4					
N(1) --H(1) ..O(10	1.00	1.88	2.8802	179	1+x,y,z
O(7) --H(11) ..O(10)	0.84	2.12	2.8752	150	1+x,y,z
N(2) --H(11A) ..O(2)	1.00	1.95	2.9103	161	2-x,1/2+y,1-z
O(9) --H(13A) ..O(1)	0.93	2.6	3.3229	135	2-x,1/2+y,1-z
O(9) --H(13A) ..O(2)	0.93	1.94	2.8563	169	2-x,1/2+y,1-z
O(9) --H(13B) ..O(5)	0.77	2.09	2.8344	160	1+x,y,z
O(8) --H(14) ..O(2)	0.84	2.2	2.9195	143	2-x,1/2+y,1-z
O(10) --H(15A) ..O(4)	0.84	1.91	2.7383	168	
C(4) --H(3B) ..O(8)	0.99	2.59	3.3357	132	1-x,-1/2+y,1-z
C(17) --H(12) ..O(1)	0.95	2.33	3.0902	137	
7					
O(4) -H(19)..O(2)	0.84	1.84	2.680(15)	173	1/2-x,1/2+y,1-z
C(11)-H(11) ..O(4)	0.95	2.39	3.218(15)	146	1/2-x,1/2+y,1-z
C(14)-H(14) ..O(5)	0.95	2.56	3.50(2)	171	-x,y,1-z
8					
N(2) --H(4) ..O(1)	0.98	2.35	3.1447	137	1/2-x,-1/2+y,1-z
O(6) --H(6) ..O(3)	0.82	1.88	2.7	176	1/2-x,-1/2+y,2-z
C(5) --H(5) ..O(6)	0.93	2.43	3.2147	143	1/2-x,1/2+y,1-z
C(12) --H(12) ..O(3)	0.98	2.58	3.475	152	1/2-x,1/2+y,2-z
C(16) --H(16A) ..O(3)	0.96	1.8	2.7488	168	1/2-x,1/2+y,2-z
9					
O(3) --H(3) ..O(7)	0.82	1.94	2.6711	147	1/2-x,1/2+y,1-z
C(2) --H(2A) ..O(8)	0.93	2.28	3.104	147	
C(16) --H(16A) ..O(1)	0.96	2.31	3.1401	144	1/2-x,-1/2+y,1-z
C(17) --H(17A) ..O(8)	0.96	2.35	3.2791	163	
C(17) --H(17B) ..O(1)	0.96	2.57	3.3068	133	
C(17) --H(17C) ..O(1)	0.96	2.28	3.1928	159	1/2-x,1/2+y,1-z
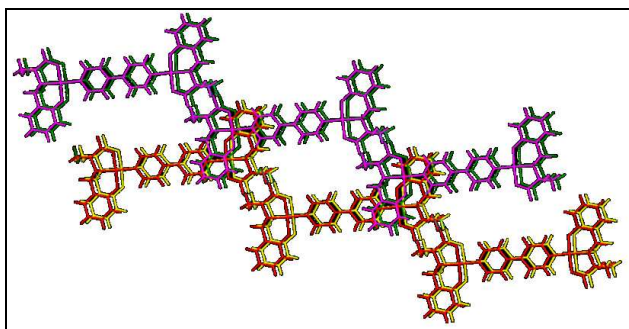
Fig. 7 Overlap of 1st with 3rd and 2nd with 4th layers in 2D supramolecular layers in **7**.

Similarly in **8**, the strong intermolecular hydrogen bonding between the uncoordinated oxygen atom (O3) of the monodendate carboxylate and the oxygen atom (O6) of the CH_2OH (O---O distance: 2.70 Å) of the ligand of next asymmetric unit gives rise to a supramolecular network of $[Cu_2(4,4'-bpy)(Hser-5-Cl-sal)_2]\cdot H_2O$ with pores (see Figs. 8a and 8b) having dimensions 19.095 Å x 6.805 Å.
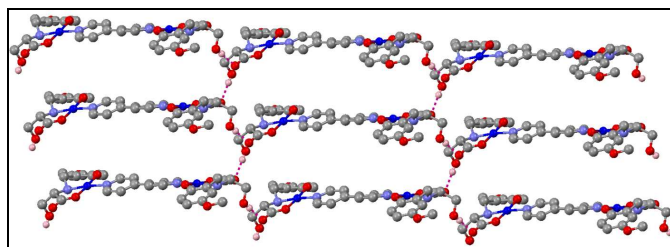
Fig. 8a Perspective view of the 2D supramolecular assembly in **8**.
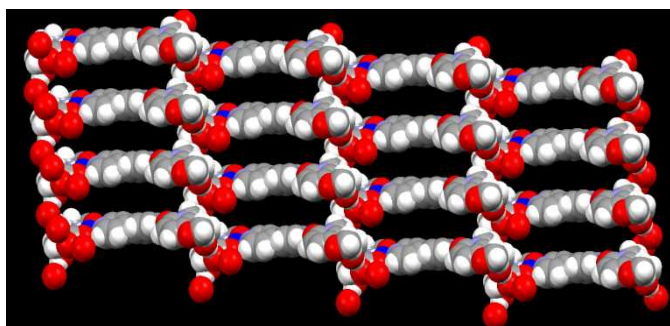
Fig. 8b Space fill representation of the supramolecular assembly in **8**.

Compound **9** crystallizes in the same chiral space group (C2) as **7** and **8** and its asymmetric unit (as shown in Fig. 9) is similar to those of **7** and **8** except **9** has three lattice DMSO molecules instead of lattice water molecules found in **7** and **8**. No supramolecular assembly is observed in **9** as the hydrogen bonding exists between the oxygen atom (O3) of the $-CH_2OH$ of the ligand and the oxygen atom (O7) of one of the lattice DMSO molecules (O---O distance: 2.671 Å) (see Fig. S7, ESI), thus preventing O3 to do any further hydrogen bonding with the oxygen atom of the carboxylate of the next molecule. Hydrogen bonding parameters for **7**, **8** and **9** are summarized in Table 2.
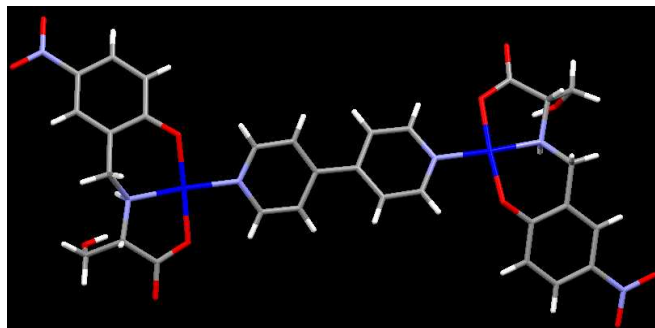
Fig. 9 Asymmetric unit in **9** (lattice DMSO molecules are omitted for clarity).

Powder X-ray data analysis. To confirm whether the single crystal structure corresponds to the bulk material or not, powder X-ray diffraction patterns were recorded for **1**, **4**, **7**, **8** and **9** at room temperature. The experimental and simulated (from the single crystal data) patterns were similar to each other (see Fig. S8-S12, ESI). The patterns obtained confirm that the single crystal and bulk material are the same. It also confirms the phase purity of the bulk sample. Additionally, powder patterns of **1** and **7** after drying at 100 °C for 15 minutes were recorded. In each case, there is no change in the powder pattern indicating the retention of structure and crystallinity due to this treatment. In addition to showing that compound **1** can be prepared at room temperature or under reflux conditions (see the 'Experimental Section') the finding from the PXRD experiment indicates that it does not go through any structural transformation due to heating in the liquid or solid state. This also corroborates well with their thermal properties which is described below.

Conversion of CPs to SCCs. Just considering the bonds broken in **1** and bonds formed in **7** (Scheme 1) it is very clear that it is not a *simple ligand exchange reaction*. First, the bis(phenoxo)dicopper core in **1** is very stable (Cu-O bonds are symmetrical) and thus inserting the neutral 4,4'-bpy ligand between the two Cu(II) centers to form **7** requires changing the bridging mode of the phenoxo groups to the monodendate mode. Secondly, during this transformation reaction the binding modes of both the $-CH_2OH$ and $-CO_2^-$ groups in the Sersal ligand are also affected showing a lot of changes around the copper centers in the polymeric structure of **1**. This can be understood by observing the change in the coordination numbers of the metal centers (Cu1: 6 to 4 and Cu2: 5 to 4) during this transformation. The strong hydrogen bonding between the dinuclear subunits in **7** that stabilized it over **1** should be considered. Even though a coordination polymer (CP) is considered to be a more stable than the networks of a dinuclear complex, different bindings of the functionalities of the same ligand as well as strong hydrogen bonding are responsible for such transformation. It should be noted that based on the PXRD data the bulk of **7** (in high yield) is same as its crystals used in structure determination removing any doubt

that kinetic artefact of crystal growth could be the reason for its formation instead of thermodynamic end product. This is an unexpected finding and questions the strength of coordination bonds in polymeric structures. There is no prior example in the literature for such transformation as mentioned in the 'Introduction' section. In fact, a *simple ligand exchange reaction* (substituting the water molecule on Cu2) to connect the 2D CP of **1** with the 4,4'-bpy ligand would have given an expected product.

FT-IR and Raman spectroscopy. The IR spectra of **1-6** (see Figs. S13-S22, ESI) recorded in the solid state as KBr pellets are similar but with slight shifts in some band positions. As an example, for **1** a broad band at 3400 cm^{-1} corresponds to the O-H stretching frequency of the –CH_2-OH of the ligand which is coordinated to the Cu(II) and the N-H stretching frequency appears at 3233 cm^{-1}. Two binding modes of the carboxylate group of the ligand (monodentate and bridged) observed in the crystal structure of **1** are in agreement with the presence of two types of asymmetric and symmetric stretches for the -COO^- groups in **1**. These values are 1613 cm^{-1} and 1486 cm^{-1}, and 1581 cm^{-1} and 1363 cm^{-1}, respectively, corresponding to $\Delta\upsilon_1 = 127$ cm^{-1} (bridged) and $\Delta\upsilon_2 = 218$ cm^{-1} (monodentate) [where $\Delta\upsilon = \upsilon_{asym} - \upsilon_{sym}$]. The C-O stretching for the phenoxo part of the ligand, which is bridging between the two Cu(II) centers, appears at 1276 cm^{-1}. The corresponding values for **2-6** along with those for **1** are listed in Table S3, ESI. All these IR values for **1-6** are in well accordance with the similar dimeric compounds known in the literature.[16-18,21] Similarly, the IR spectra for **7-10** are similar (see Table S4, ESI). As an example, for **7** the O-H stretching frequency of the –CH_2-OH of the ligand and the N-H stretching frequency appear at 3355 cm-1 and 3196 cm^{-1}, respectively. 1479 cm^{-1} for **7**, 1495 cm^{-1} for **8**, 1477 cm^{-1} for **9** and 1473 cm^{-1} for **10**. In **1**, **2**, **3**, **4**, **5**, **6**, **7**, **8**, **9** and **10**, , 1268 cm^{-1}, 1303 cm^{-1}, 1267 cm^{-1}, 1280 cm^{-1}, 1267 cm^{-1}, 1276 cm^{-1}, 1272 cm^{-1}, 1290 cm^{-1} and 1287 cm^{-1}, respectively. The peak at 1217 cm^{-1} in **7**, **8** and **9**, and 1219 cm^{-1} in **10** is from 4,4'-bipyridine.[31] The corresponding values for **8-10** along with those for **7** are listed in Table S4, ESI.

In the Raman spectra of **1**, **2**, **3**, **4**, **5** and **7**, the peak corresponding to the carboxylate stretching appears at 1638 cm^{-1}, 1615 cm^{-1}, 1603 cm^{-1}, 1599 cm^{-1}, 1592 cm^{-1} and 1624 cm^{-1}, respectively. The peak at 1282 cm^{-1} for **1**, 1310 cm^{-1} for **2**, 1297 cm^{-1} for **3**, 1283 cm^{-1} for **4**, 1278 cm^{-1} for **5** and 1300 cm^{-1} for **7** corresponds to the N-H bend of the ligand (see Fig. S23 of the ESI).

UV-Vis and Circular Dichroism (CD) spectroscopy. UV-Visible and CD spectroscopic studies were carried using ~1 mM methanolic solution of **1-10** (see Figs. 10a, 10b, 11a and 11b). The UV-Vis spectral data for **1-10** are reported in Tables S5-S6 of the ESI. The peaks around 650-685 nm in these complexes are due to the d-d transition (^2E_g to $^2T_{2g}$) of copper(II) whereas the peaks around 370-420 nm are due to LMCT, i.e., from -C=O of carboxylate to the metal center.[32] These values for **1-6** are in well agreement with corresponding

values for such phenoxo bridged Cu(II) compounds known in literature.[20,21,26] In the UV region of the spectrum (200 to 350 nm), the peaks at around 200-210 nm (π-π*) is due to L-serine part of the ligand and 245-260 nm (n-π*) is due to aldehyde part of the ligand. In **7**, **8**, **9** and **10**, a peak at around 235 nm for 4,4'-bipyridine (π-π*) is also observed.

The peaks in the CD spectra for **1-10** are reported in Tables S7-S8 of the ESI†. The Cotton effects observed at around 400 are due to LMCT whereas the Cotton effects observed around 650 nm are due to d-d transitions.[33]
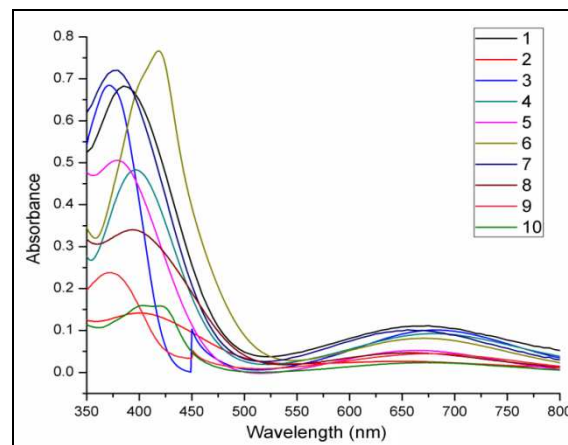
Fig. 10a UV-vis spectra for **1-10** in wavelength range from 350 to 800 nm.
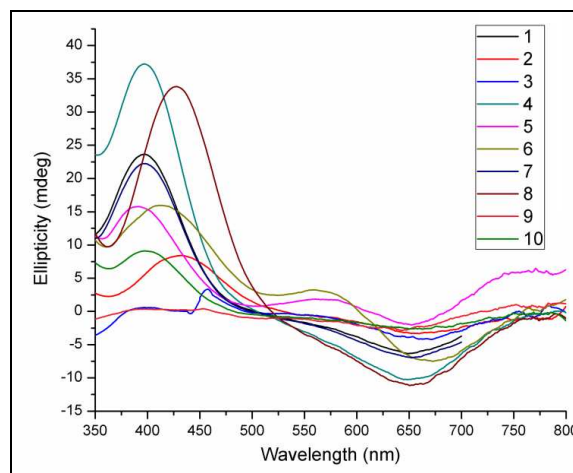
Fig. 10b CD spectra for **1-10** in wavelength range from 350 to 800 nm.

Thermogravimetric analyses. The thermal stability of **1-10** was studied as a function of temperature in the range of 25-500 ˚C. In all CPs **1-6**, it is a two step weight loss profile (see Fig. 12). The first weight loss in all the cases at ~50-200 °C is due to loss of lattice solvents and in some (**1**, **4** and **5**) loss of coordinated solvent took place as well. The next loss above 200 °C in all CPs is due to loss of the organic ligand and the remaining coordinating solvent if any. The exact %loss values for **1-6** are reported in Table S9 of the ESI†.
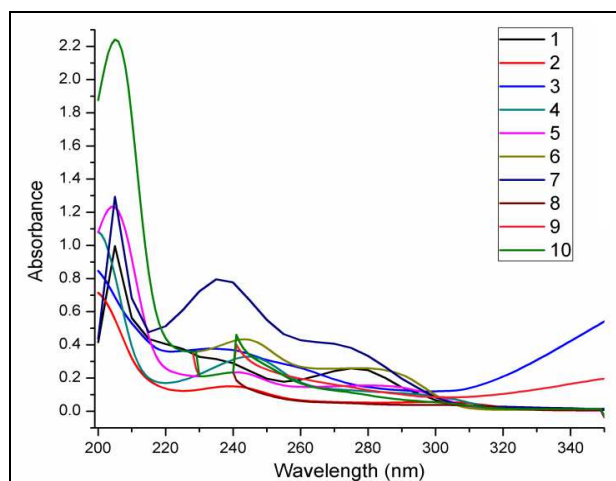
Fig. 11a UV spectra for **1-10** in wavelength range from 200 to 350 nm.
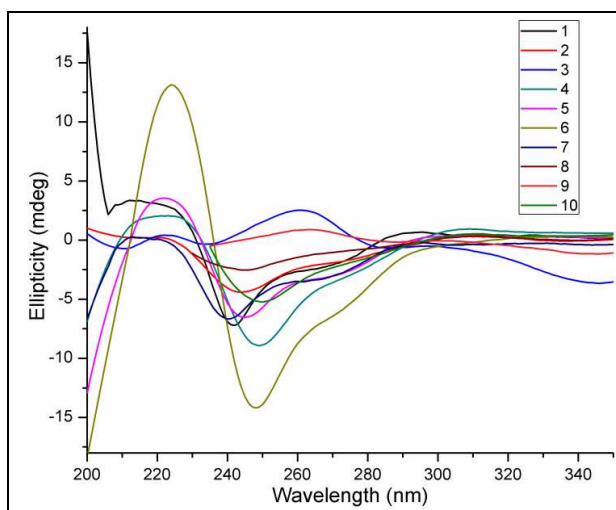
Fig. 11b) CD spectra for **1-10** in wavelength range from 200 to 350 nm.

For **7-10**, it is a three step weight loss profile (see Fig. 13). The first weight loss (~ 50-150 °C) in almost all cases is due to loss of uncoordinated solvent molecule, the second weight loss (~ 150-300 °C) is due to loss of remaining uncoordinated solvent and bipyridine molecule and the third weight loss (~ 300-500 °C) is due to loss of the remaining organic part of the complex. The exact % loss values for 7-10 are reported in Table S10 of the ESI†.

Magnetic properties. For comparison, variable-temperature magnetic susceptibility measurements were performed on powdered samples of **1** and **7** in the temperature range 2-380 K. The plot of the observed magnetic susceptibility (χ_{obs}) versus temperature (T) including best fit theoretical line for **1** is shown in the inset of Fig. 14. The observed susceptibility (χ_{obs}) shows a broad maximum at around 200–250 K before decreasing at lower temperatures. Below about
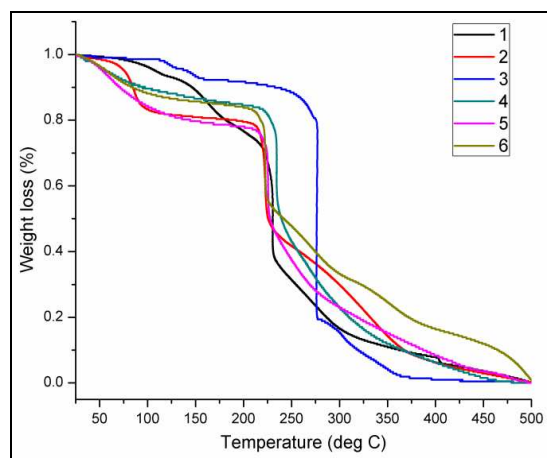
Fig. 12 TGA Scans for **1-6**.
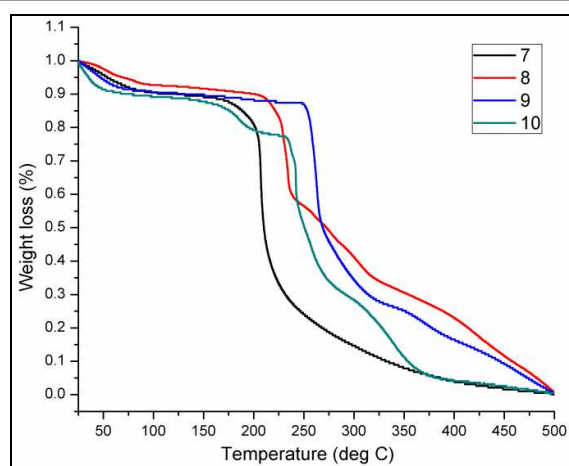
Fig. 13 TGA Scans for **7-10**.

20 K, χ_{obs} increases strongly. This lowest temperature behavior most likely arises from the presence of a small amount of paramagnetic impurities in the material. The plot of χT versus T for **1** is shown in Fig. S24 of the ESI. As expected, the value of χT is much lower than expected (0.375 cm³/Cu mol) for free S = ½ moments with a g-factor of 2. This reduction is due to the fact that at 400 K the Cu(II) spins with S = ½ are already coupled antiferromagnetically. The χT continues to decrease with lowering T and goes to 0 as T tends to 0 as expected for a spin-singlet state of dimerized spins. The magnetic susceptibility of S = ½ dimers should have the following temperature dependence based on the modified Bleaney-Bowers equation[34]:

$$\chi_{dimer} = \frac{3C/_T}{\left(3 + exp\left(\frac{\Delta}{T}\right)\right)}$$

where C is the Curie constant for S = ½ moments and Δ is the spin-gap produced by phenoxo-bridged dicopper units. Δ is also the strength of the magnetic interaction (Δ = -2J, where J is the antiferromagnetic exchange given by the nearest-neighbor Heisenberg Hamiltonian $H = -2JS_1.S_2$) between the S = ½

moments. The χ_{obs} therefore has two contributions - the intrinsic contributions from the strongly coupled dicopper units and the paramagnetic impurity contribution - as follows:

$$\chi_{imp} = \chi_0 - \frac{C_{imp}}{T - \theta}$$

where χ_0 is a temperature independent contribution, C_{imp} is the Curie constant of the impurity and θ is the Weiss temperature associated with interactions between these impurities. Thus, the χ_{obs} was fitted by the expression $\chi_{obs} = \chi_{imp} + \chi_{dimer}$. The main panel in Fig. 14 shows the dimer susceptibility after the impurity part has been subtracted; the solid curve through the data is the theoretically expected χ_{dimer} for S = ½ dimers. An excellent fit was obtained as shown by the solid curve through the χ_{obs} data in the inset with the following values: $C_{imp} = 0.009$ cm^3/Cu mol K, $\theta = -4.7$ K, C = 0.51 cm3/Cu mol K, $\Delta = 400$ K. In terms of the exchange interaction, $-2J = 400$ K = 278 cm^{-1}. This value is in the range observed for the bis(phenoxo) bridged square pyramidal Cu(II) dimers in CPs[16] or discrete compounds providing an excellent magneto-structural correlation (2J value versus Cu(II)-O-Cu(II) angle and Cu(II)...Cu(II) distance).[35-37]
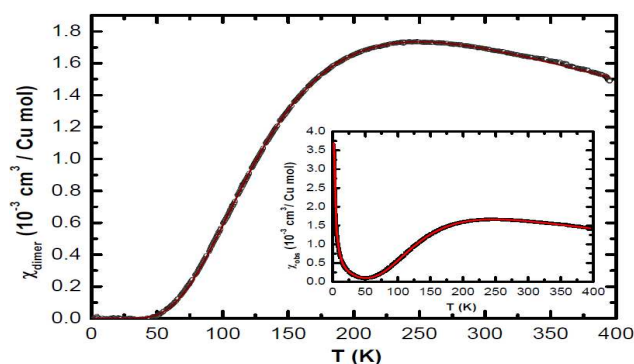
Fig. 14 χ_{dimer} vs T plot for **1**; the solid line is the best fit to the experimental data. Inset: χ_{obs} vs T plot.

In contrast, based on the structure of **7** for non-interacting Cu(II) ions (independent S = ½ moments) a Curie-Weiss like paramagnetic behavior is expected in the whole temperature range. This is exactly what is observed in magnetic measurements. Figure 15 shows the χT versus T data between 2-390 K. The value at 390 K is 0.375 cm^3/Cu molK, which is close to the value expected for S = ½ moments. The χT has weak T dependence down to the lowest temperatures and its value stays close to the expected free spin S = ½ value. The inset shows the inverse susceptibility 1/χ versus T data. The data could be fit using a Curie-Weiss expression:

$$\chi = \chi_0 + \frac{C}{T - \theta}$$

The fit shown as the solid curve through the data gave the values $\chi_0 = -3.8 \times 10^{-5}$ cm^3/Cu mol, C = 0.35 cm^3/Cu molK, and $\theta = 0$ K. The obtained value of the Curie constant C is slightly lower than but close to the expected value 0.375 cm^3/Cu molK expected for S = ½ moments with a g-factor of 2. The $\theta = 0$

indicates that the Cu(II) centers bridged by the 4,4'-bpy ligand do not interact at all.
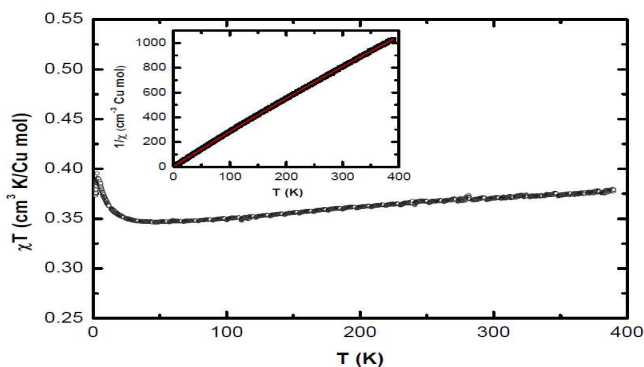
Fig. 15 χT vs T plot for **7**; the solid line is the best fit to the experimental data. Inset: 1/χ vs T plot.

Water adsorption studies. In order to demonstrate the change in the porous nature of **7-10** compared to **1-6**, in the solid state structures described above, as an example water adsorption studies of **1** and **7** were carried out. Each sample of **1** and **7** was pretreated for 24 hours at 100 °C under vacuum followed by purging with nitrogen to use in this study. At p/p$_o$ = 1 (where po is the vapor pressure at saturation), **1** adsorbed approx. 340 cm^3 water per g of sample with very little at low p/p$_o$ value (see Fig. 16). The least affinity towards water by **1** correlates well with its structure. On the other hand, **7** adsorbed approx. 220 cm^3 water per g of sample in a gradual uptake (see Fig. 16). This value indicates a strong adsorbate-adsorbate interactions via hydrogen bonding at higher p/p$_o$. Its desorption curve does not follow the adsorption one generating a prominent hysteretic profile that is indicative of hydrophilic nature of the pore surfaces in it. On desorption it showed retention of water confirming the fact that at ambient conditions it retains two-third of the water upon rehydration. This study clearly indicates the porous nature of **7**.
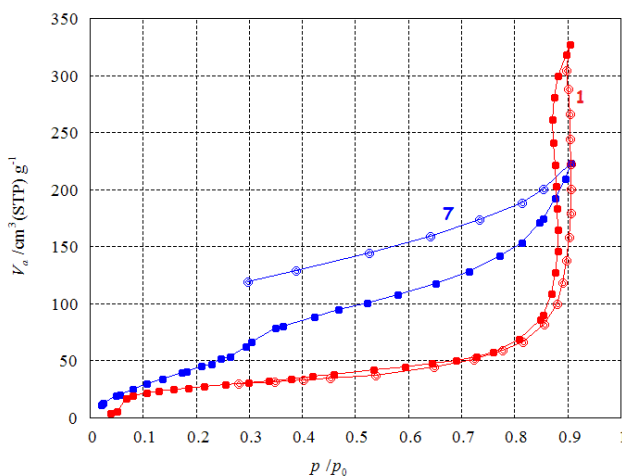
Fig. 16 Water adsorption isotherms for **1** and **7** (Redlines: **1**, Bluelines: **7**; filled squares, adsorption and circles, desorption).

Conclusions

In this article we have reported the one-pot synthesis, which includes a very simple yet effective work-up affording pure compounds in high yields without any further purification steps, of a series of 2D CPs $\{[Cu_2(Hsersal)_2(H_2O)]\cdot H_2O\}_n$ (**1**), $\{[Cu_2(Hser-5OMe-sal)_2(H_2O)]\cdot DMF\}_n$ (**2**), $\{[Cu_2(Hser-5NO_2-sal)_2(H_2O)]\cdot 2H_2O\}_n$ (**3**), $\{[Cu_2(Hser-5Cl-sal)_2(H_2O)]\cdot H_2O\}_n$ (**4**), $\{[Cu_2(Hser-3Cl-sal)_2(H_2O)]\cdot 3H_2O\}_n$ (**5**) and $\{[Cu_2(Hser-o-Van)_2(H_2O)]\cdot 3H_2O\}_n$ (**6**). Some of these CPs are converted to SCCs, $[Cu_2(4,4'-bpy)(Hsersal)_2]\cdot 2H_2O$ (**7**), $[Cu_2(4,4'-bpy)(Hser-5-OMe-sal)_2]\cdot 6H_2O$ (**8**), $[Cu_2(4,4'-bpy)(Hser-5-NO_2-sal)_2]\cdot H_2O$ (**9**) and $[Cu_2(4,4'-bpy)(Hser-5-Cl-sal)_2]\cdot 4H_2O\cdot DMF$ (**10**). An extensive characterization of these CPs and SCCs by elemental analysis, IR and Raman spectroscopy, electrospray mass spectrometry, single crystal and powder X-ray diffraction, polarimetry, UV-vis and circular dichroism spectroscopy, and thermogravimetric analysis has provided their structural similarities and differences as well as spectroscopic and thermal properties. Based on the variable temperature magnetic susceptibility measurements between 2-380 K, strong antiferromagnetic coupling ($2J = -278$ cm^{-1}) for **1** and no interaction for **7** between the Cu(II) centers are observed. Finally, the affinity towards water based on the water adsorption study by **1** and **7** is highly correlated to their formation; the dynamic behaviour and soft nature of **7** established in this study is of great interest for further studies. The current work has thus laid the foundation for the strategy in developing new pairs with other bifunctional linkers. Based on the results presented here, further work continues in our laboratory to understand the effect of the change in the ancillary ligands and other metal centers.

Acknowledgements

Notes

[a]Department of Chemical Sciences and [b]Department of Physical Sciences, Indian Institute of Science Education and Research, Mohali, Sector 81, Manauli PO, S.A.S. Nagar, Mohali, Punjab 140306, INDIA
*e-mail: sanjaymandal@iisermohali.ac.
[¶]Current address: Department of Chemistry, DAV University, Jalandhar, Punjab 144001, INDIA

†**Electronic supplementary information (ESI) available:** Crystallographic data of the structures **1**, **4**, **7**, **8**, and **9** in CIF format (CCDC 952777, 981858, 952778, 981859, 981860, respectively). Additional figures related to X-ray crystallography for these species (Figs. S1−S7), PXRD patterns (Figs. S8-S12), FTIR and Raman spectra (Figs. S13-S23), Magnetic data for **1** (Fig. S24) and selected bond distances and angles of **1**, **4**, **7**, **8** and **9** (Tables S1-S2), selected FTIR stretching frequencies for **1-10** (Tables S3-S4), UV-vis spectral data for **1-10** (Tables S5-S6), CD spectral data (Tables S7-S8) for **1-10** and TGA data for **1-10** (Tables S9-S10).

References

1. J. J. Wolff, *Angew. Chem. Int. Ed. Engl.*, 1996, **35**, 2195.

2. J. M. Lehn, *Supramolecular Chemistry: Concepts and Perspectives*, VCH: New York, 1995.

3. N. L. Rosi, J. Kim and O. M. Yaghi, *J. Am. Chem. Soc.*, 2005, **127**, 1504.

4. J. W. Steed and J. L. Atwood, *Supramolecular Chemistry*, John Wiley & sons, Ltd.: New York, 2009.

5. (a) C. N. R. Rao, S. Natarajan and R. Vaidhyanathan, *Angew. Chem. Int. Ed.,* 2004, **43**, 1466; (b) E. B. Bauer, *Chem. Soc. Rev.,* 2012, **41**, 3153; (c) W. Xuan, M. Zhang, Y. Liu, Z. Chen and Y. Cui, *J. Am. Chem. Soc.*, 2012, **134**, 6904.

6. A. D. Burrows, C. W. Chan, M. M. Chowdhry, J. E. McGrady and D. M. P. Mingos, *Chem. Soc. Rev.*, 1995, **24**, 329.

7. L. Brammer, in *Perspective in Supramolecular Chemistry - Crystal Design: Structure and Function; G. R. Desiraju, Ed.,* Wiley: England, 2003; Vol. 7, p 1-75.

8. A. M. Beatty, *CrystEngComm*, 2001, **3**, 243.

9. C. B. Aakeroy and A. M. Beatty, *Aust. J. Chem.*, 2001, **54**, 409.

10. G. R. Desiraju, *J. Chem. Soc., Dalton Trans.*, 2000, 3745.

11. S. Subramanian and M. J. Zaworotko, *Coord. Chem. Rev.*, 1994, **137**, 357.

12. B. Wisser, A. C. Chamayou and R. Miller, *CrystEngComm*, 2008, **10**, 461.

13. B. Wisser, Y. Lu and C. Jainak, *Z. Anorg. Allg. Chem.*, 2007, **633**, 1189.

14. L. F. Ma, L. Y. Wang and J. G. Wang, *Z. Anorg. Allg. Chem.*, 2006, **632**, 487.

15. (a) R. Ganguly, B. Sreenivasulu and J. J. Vittal, *Coord. Chem. Rev.*, 2008, **252**, 1027; (b) J. J. Vittal, *Coord. Chem. Rev.*, 2007, **251**, 1781.

16. C. T. Yang, M. Vetrichelvan, X. Yang, B. Moubaraki, K. S. Murray and J. J. Vittal, *Dalton Trans.*, 2004, 113.

17. J. D. Ranford, J. J. Vittal and D. Wu, *Angew. Chem. Int. Ed.,* 1998, **37**, 1114.

18. J. D. Ranford, J. J. Vittal, D. Wu and X. Yang, *Angew. Chem. Int. Ed.*, 1999, **38**, 3498.

19. J. D. Ranford, J. J. Vittal, D. Wu and X. Yang, *Cryst. Growth Des.*, 2005, **5**, 41.

20. X. Yang, J. D. Ranford and J. J. Vittal, *Cryst. Growth Des.*, 2004, **4**, 781.

21. M. Nagarathinam, K. Saravanan, W. L. Leong, P. Balaya and J. J. Vittal, *Cryst. Growth Des.*, 2009, **9**, 4461.

22. S. Khullar and S. K. Mandal, *Cryst. Growth Des.*, 2012, **12**, 5329.

CrystEngComm Accepted Manuscript

23. *APEX2*, *SADABS* and *SAINT*, Bruker AXS Inc, Madison, WI, USA, 2008.

24. G. M. Sheldrick, *Acta Crystallogr., Sec. A: Found. Crystallogr.*, 2008, **A64**, 112.

25. C. F. Macrae, I. J. Bruno, J. A. Chisholm, P. R. Edginton, P. McCabe, E. Pidocck, L. Rodriguez-Monge, T. Taylor, J. Van de Streek and P. A. Wood, *J. Appl. Crystallogr.,* 2008, **41**, 266.

26. A. L. Spek, *PLATON, Version 1.62*, University of Utrecht, 1999.

27. K. Biradha, *CrystEngComm*, 2003, *5*, 374.

28. W. T. Guo, Z. M. Mio and Y. L. Wang, *Z. Naturforsch.,* 2012, **67**, 774.

29. B. Y. Lou and M. C. Hong, *Acta Cryst.,* 2008, **E64**, 405.

30. R. Karmakar, C. R. Choudhury, S. Mitra and L. Dahlenburg, *Struct. Chem.,* 2005, **16**, 6.

31. K. Nakamoto, *Infrared Spectra of Inorganic and Coordination Compounds Part B. 5th Ed.*, John Wiley & Sons: New York, 1997.

32. T. M. Dunn, in *The visible and ultraviolet spectra of complex compounds in modern coordination chemistry*, Interscience: New York, 1960.

33. K. Nakanishi, N. Berova and R. W. Woody, *Circular Dichroism: Principles and Applications*, VCH: New York, 1994.

34. B. Bleaney and K. D. Bowers, *Proc. R. Soc. London, Ser. A*, 1952, **214**, 451.

35. S. K. Mandal, L. K. Thompson, M. J. Newlands, E. J. Gabe and K. Nag, *Inorg. Chem.*, 1990, **29**, 1324.

36. R. Gupta, S. Mukherjee and R. Mukherjee, *J. Chem. Soc., Dalton Trans.*, 1999, 4025.

37. H. Saimiya, Y. Sunatsuki, M. Kojima, S. Kashino, T. Kambe, M. Hirotsu, H. Akashi, K. Nakajima and T. Tokii, *J. Chem. Soc., Dalton Trans.,* 2002, 3737.

Table of contents – artwork and synopsis
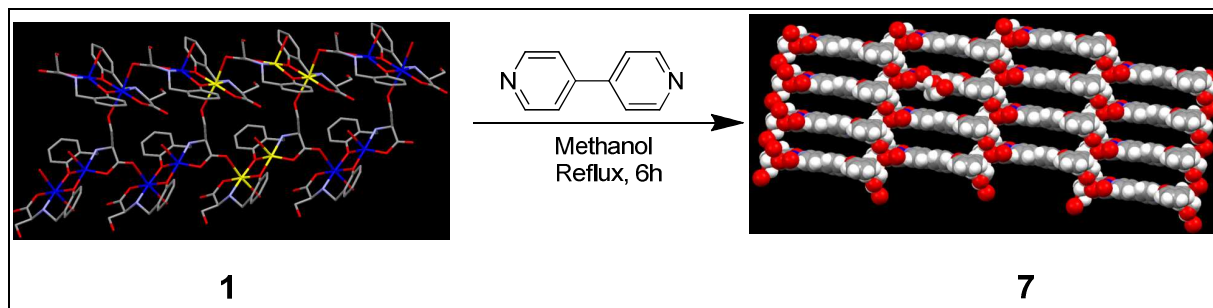
Formation of 2D homochiral coordination polymers and the corresponding homochiral 2D supramolecular assemblies using 4,4'-bipyridine as a bifunctional linker: for example, $\{[Cu_2(HSersal)_2(H_2O)]\cdot H_2O\}_n$ (**1**), (where $H_3sersal$ = N-(2-hydroxybenzyl)-serine), to $[Cu_2(4,4'\text{-bpy})(Hsersal)_2]\cdot 2H_2O$ (**7**) via hierarchical coordination-driven self-assembly and hydrogen bonding interfaces. Their structural characterization by various analytical techniques including single crystal X-ray diffraction, magnetic properties and water adsorption studies are reported.

CrystEngComm Accepted Manuscript